

Engineered Silicon Carbide Three-Dimensional Frameworks through DNA- Prescribed Assembly

A. Michelson, O. Gang

To be published in "Nano Letters"

February 2021

Center for Functional Nanomaterials
Brookhaven National Laboratory

U.S. Department of Energy
USDOE Office of Science (SC), Basic Energy Sciences (BES) (SC-22)

Notice: This manuscript has been authored by employees of Brookhaven Science Associates, LLC under Contract No. DE-SC0012704 with the U.S. Department of Energy. The publisher by accepting the manuscript for publication acknowledges that the United States Government retains a non-exclusive, paid-up, irrevocable, world-wide license to publish or reproduce the published form of this manuscript, or allow others to do so, for United States Government purposes.

DISCLAIMER

This report was prepared as an account of work sponsored by an agency of the United States Government. Neither the United States Government nor any agency thereof, nor any of their employees, nor any of their contractors, subcontractors, or their employees, makes any warranty, express or implied, or assumes any legal liability or responsibility for the accuracy, completeness, or any third party's use or the results of such use of any information, apparatus, product, or process disclosed, or represents that its use would not infringe privately owned rights. Reference herein to any specific commercial product, process, or service by trade name, trademark, manufacturer, or otherwise, does not necessarily constitute or imply its endorsement, recommendation, or favoring by the United States Government or any agency thereof or its contractors or subcontractors. The views and opinions of authors expressed herein do not necessarily state or reflect those of the United States Government or any agency thereof.

Engineered silicon carbide three-dimensional frameworks through DNA-prescribed assembly

Aaron Michelson¹, Honghu Zhang², Shuting Xiang³, Oleg Gang^{1,2,3}*

¹Department of Applied Physics and Applied Mathematics, Columbia University, New York, NY, 10027 USA

²Center for Functional Nanomaterials, Brookhaven National Laboratory, Upton, NY, 11973 USA

³Department of Chemical Engineering, Columbia University, New York, NY, 10027 USA

E-mail: og2226@columbia.edu

Keywords: Silicon carbide, DNA nanotechnology, self-assembly, molecular templating, nano-architectures

Abstract:

The ability to create nano-engineered silicon carbide (SiC) architectures is important for the diversity of optical, electronic and mechanical applications. Here we report a fabrication of periodic three-dimensional (3D) SiC nanoscale architectures using a self-assembled and designed 3D DNA-based framework. The assembly is followed by the templating into silica and subsequent conversion into silicon carbide using a lower temperature pathway (<700°C) via magnesium reduction. The formed SiC framework lattice has a unit size of about 50nm and domains over 5 um, and it preserves the integrity of the original 3D DNA lattice. The spectroscopic and electron microscopy characterizations reveal SiC crystalline morphology of 3D nano-architected lattices, while electrical probing shows two orders of magnitude enhancements of electrical conductivity over the precursor silica framework. The reported approach offers a versatile methodology towards creating highly structured and spatially prescribed SiC nano-architectures through the DNA-programmable assembly and the combination of templating processes.

1. Introduction:

Nanostructured silicon carbide (SiC) has attracted much attention due to the potential applications related to their excellent mechanical strength, chemical stabilities, optical and electronic properties.¹⁻⁶ Particularly, nano-architected Si and SiC are active areas of exploration in the fields of photovoltaics and optoelectronics. For example, due to the stability of the SiC bond and its wide (>3 eV) band gap, it is suitable for high temperature operation in devices.⁷⁻¹⁰ Mechanically, silicon carbide is a high strength material, which has been shown to enhance the strength of composite materials when incorporated into the nanostructure of nanowires and as a silicon substitute in microelectromechanical systems (MEMS).¹¹⁻¹³ Precisely formed 3D nanoscale architectures also holds enormous potential for engineering of nano-porous materials, with mechanical, electromechanical, mass transport and optical applications.¹⁴⁻¹⁷ Particularly with respect to optical and photonic applications, the high refractive index of silicon carbide and silicon in comparison to silica drives the need to create tailorable 3D synthesis pathways to enable fabrication of complexly designed photonic devices.^{5,6,18}

Although low dimensional, 1D and 2D, nanostructures of SiC can be fabricated with a help of traditional nanofabrication methods, the ability to create engineered 3D SiC-based nanomaterials is quite limited. One of the major obstacles to advancing the study on properties of SiC-based nanostructures and devices and transference to applications is the lack of methodology for a controllable fabrication of 3D nanoscale SiC architectures. This barrier is further hindered by the requirement for the high temperature synthesis, which generally exceeds 1400 °C.¹⁹ Recently, studies have demonstrated that both silicon and silicon carbide can be derived by magnesium reduction of a silica precursor at lower temperature (~ 650 °C) in the bulk form, there is an increasing interest to fabricate the prescribed 3D nanostructures.²⁰⁻²²

The prevalent capabilities to form patterned nanostructure of silicon and silicon carbide use top-down approaches leverage carbothermal reduction, high temperature chemical vapor deposition (CVD), plasma assisted CVD, or rf/laser/plasma assisted sputtering.^{19,23,24} However, these are generally limited to low-dimensional structures. Conversely, biologically inspired materials can often co-opt nature byproducts to template nanostructures, benefitting from thousands of years of natural selection. Indeed, some of the earliest work related to low temperature silicon and silicon carbide production through magnesium reduction leveraged M13 phage, diatoms and food byproducts to template silicon and SiC to investigate nanoscale properties and applications as sensors.^{22,25} An even richer library of structures is possible when considering the recent advances in self-assembly of polymers, ligands and colloids.²⁶⁻²⁸ For example, self-assembled polystyrene colloidal spheres were used to form meso-porous silicon or SiC crystals using a similar low temperature magnesium reduction approach, however with limited archetypes.^{29,30} Analogously, nanoscale phases formed by diblock copolymers phases were templated for creating scaffolds from SiC and other types of inorganic materials.^{27,31-35}

DNA-based bottom-up method nanotechnology offer a high degree of designability and tunability to control formation of nanoscale constructions.^{36,37} Recently, the development of DNA nanotechnology demonstrated an ability to encode a formation a variety of nano-architectures in 2D and 3D.^{27,38-42} Particularly, DNA origami technique which uses a long DNA paired with many short strands that promote DNA folding into a tens of nanometers scaffold with prescribed 3D shape.^{43,44} The rigid DNA nano-frames can be designed with exterior facing single stranded sequences at vertices or edges allowing for interactions between frames. By controlling an inter-frame connectivity one can direct self-assembly of the frames into larger scale ordered framework structures.^{36,37,45,46} In general, it was shown that DNA-based materials can be prepared in sizes

from microns to millimeters using different assembly strategies such as precipitation controlled, or surface promoted growth^{18,38,47-49}. Thus, by tuning the geometry of individual nano-frames, lattice constant, crystal structure and assembly conditions a symmetry and overall dimension can be in principle controlled.

Given the anionic nature of DNA, different types of charge molecules can be used to intercalate, decorate and template DNA⁵⁰⁻⁵⁵, thus opening possibilities to create a variety of organic and inorganic nanomaterial which nano- and meso-structure is dictated by the underlying rationally designed individual DNA scaffolds or scaffolds assembled into superlattices.^{37,46,53,56} The ability to template silicon carbide from such self-assembled architectures would thus open up an immense library of structures possible to utilize and explore for diverse optical, electronic and mechanical applications.

Here we present an approach for templating such superlattices into a silicon-carbide framework, which is achieved by assembly 3D lattice framework from DNA frames, lattice silication and conversion into SiC with preserved nanoscale architecture of 3D DNA framework. Using structural, spectroscopic, and electrical characterization methods, we demonstrate a successful formation of SiC superlattice, reveal its composition, and electrical properties.

2. Results/Discussion

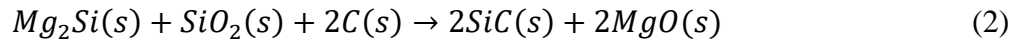
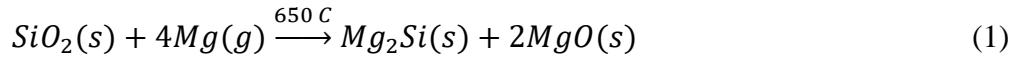
2.1 Synthesis and Magnesium Thermal Reduction

The first step for creating 3D framework is an elementary building block, the DNA frame, which can be further assembled into a superlattice. Using a DNA origami approach, an octahedron with the edge length of ~29 nm was designed and assembled, similarly to our previous studies.^{36,45} Single stranded DNA with specific sequences at vertices binds with complementary sequences on the neighboring origami frames, thus facilitating the formation of extended superlattice,

represented in **Figure 1a** (see Supplemental Material for details). The formed superlattice has a simple cubic (SC) symmetry with a lattice constant of approximately 57nm, as revealed by the small angle x-ray scattering (SAXS) characterization (Fig. S1). This larger scale DNA structure is then used for templating into inorganic nano-architected material.

We promoted a growth of silica on the ordered DNA framework using sol-gel synthesis of 3-aminopropyl-triethoxysilane (APTES) and tetraethyl orthosilicate (TEOS), Figure 1a-b, as described in supporting material/method section. The APTES/TEOS sol results in a growth of a 3-10 nm silica layer around the 6 helix-bundle struts of the DNA octahedron, which yields a porous lattice architecture with voids of about 10-20 nm, as shown in Figures S1 and S2. The assembled and silicate crystals exhibit a cubic morphology with edge length up to 5 μ m, which is consistent with Wulff shape of a SC lattice with (100) type of faces (Figure 1c). The obtained silica framework retains the architecture of the DNA superlattice, presenting a replica available for further processing. The silica struts (15-20 nm in diameter) of the framework represents the precursor for conversion to SiC. We induced this conversion through magnesium reduction of the silica, as shown in Figure 1c and Figure S2.

Specifically, we employed a two-step process for the conversion of silica into silica carbide, wherein the first step magnesium silicide is produced from the reaction of silica and magnesium vapor at the magnesium melting point forming a byproduct of magnesium oxide (**Equation 1**).²¹ This step is followed by a carbon-facilitated conversion of magnesium silicide and unconverted silica to form SiC, due to the presence of high levels of carbon in the DNA and residuals from buffer solution (**Equation 2**). The reaction is thermally assisted by the exothermic reaction of magnesium with silicon (Equation 1) lending itself towards this lower temperature pathway.



The melting temperature of magnesium, 650 °C, is generally used for the conversion operation, while lower temperatures results in the incomplete or inconclusive conversions.^{25,57} In our experimental setup, sample of silica-superlattices and magnesium turnings were collocated on a molybdenum boat (Figure 1a) and loaded to a tube furnace which was backfilled with Ar/H₂ and ramped to 650 °C for 3 hours. Subsequently the sample was soaked in HCl to remove excess magnesium and HF to remove excess SiO₂ remaining on the sample.

2.2 Nanostructure Characterization

We monitored the two-step conversion process described above by scanning electron microscopy with energy dispersive spectroscopy (SEM-EDS) to collect spatial and chemical information about the superlattices. Representative EDS spectra of the samples before and after conversion, presented in Figure 1e, show the ratio of the atomic percentage of silicon and oxygen which flip from over 2O:1Si (Silica) to 1O:2.5Si after the conversion (SiC) was completed. Small area electron diffraction (SAED) of the resulting superlattice, collected using scanning transmission electron microscopy (STEM) (see Supporting Materials, S4), indicates a crystalline structure of the converted material, with the diffraction peaks corresponding to the (111), (200), and (311) of cubic silicon carbide (SiC-3C), as shown in Figure 1b.²¹

Preservation of local (nanometer) and global (microns) structure, and full conversion to SiC require careful addition of magnesium to the reaction vessel in order to avoid adverse side reactions and ensure a penetration of the magnesium throughout the porous superlattice. Whereas, from Equation 1 we would expect that a simple 2:1 molar ratio of Mg to SiO₂ is required for conversion

to SiC, it was observed experimentally that for the superlattice precursor to achieve full conversion, the mass of Mg should exceed the mass of superlattice. Indeed, an excess or shortage of magnesium in the reactor would adversely affect the reaction and resulted in a structurally destructive process. For example, a 2 μ l drop cast solution of sample from a 5nM solution of superlattice sample, results in less than 1 μ g of material deposited onto the substrate. However, adding a 5 mg quantity of Mg turnings to the reaction chamber did not result in a complete conversion of the sample, as evident from Figure S3 and S10. When adding 15-20 mg of Mg, conversion would instead lead to the destruction of the superlattice structure. This later process is likely driven by an excess of Mg and the resulting formation of magnesium silicide which is reactive to HCl in subsequent cleaning steps. The initial silica thickness of framework struts, which control the degree of the porosity, also factors into to the successful conversion of the superlattice to SiC, requiring a porous network to ensure the efficient penetration of Mg gas into the structure. If the silica cladding is too thick, the structure may develop blockages, limiting a penetration into 3D architecture. When transforming to SiC, this might prevent a further conversion of the interior of the lattice structure. If, however, the silica layer is too thin, a structure may not have enough mechanical stability to survive the conversion process. In our investigation we observed silica cladding as thin as 3-4 nm was sufficient to be stable, see Figure S10 and S11 for further details. Our experiments showed that the optimal Mg mass of 7-10 mg allowed for the preservation of fine lattice structure and the overall crystal, as shown in Figures 1d and S4.

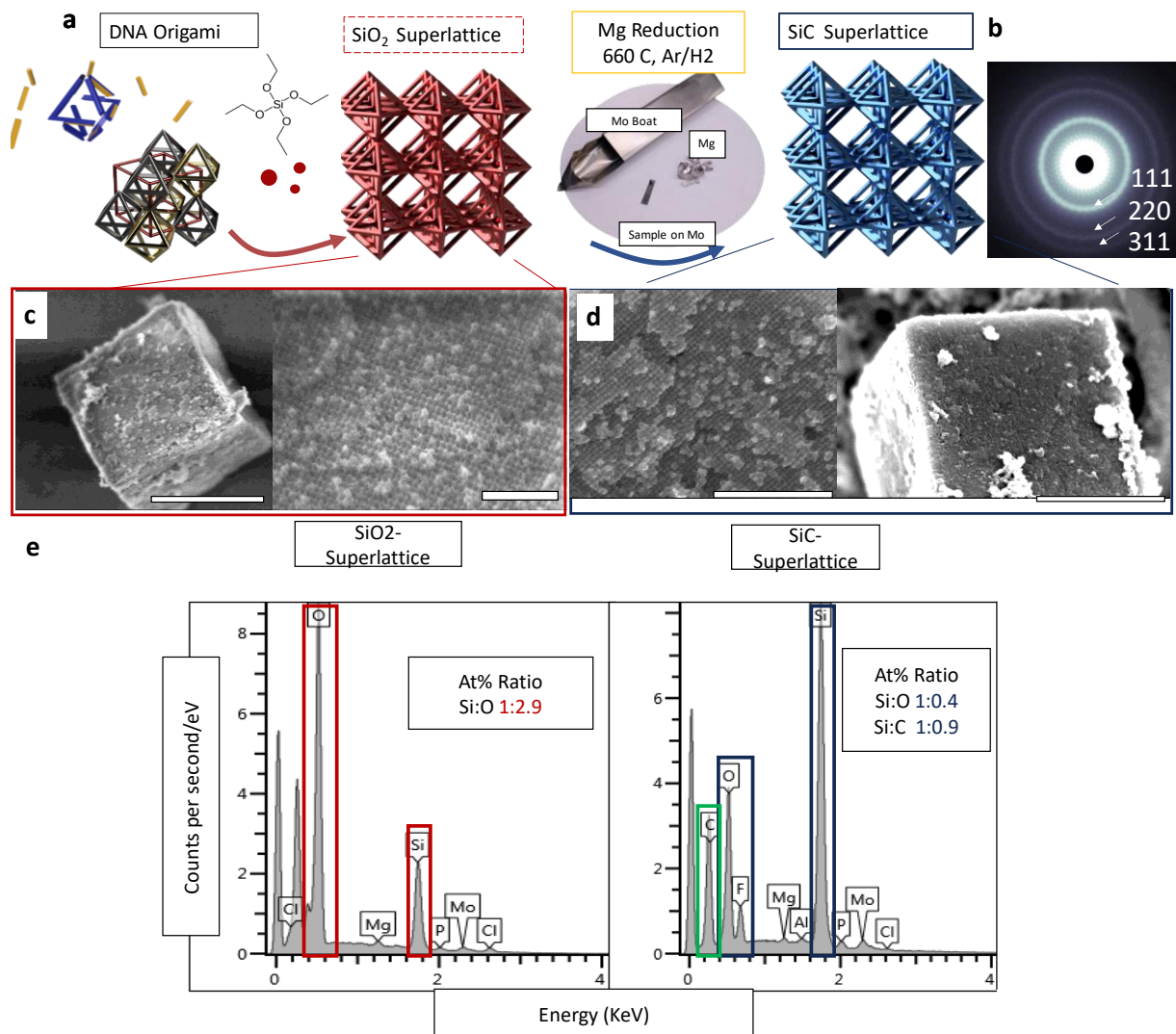


Figure 1. Synthesis of Silicon Carbide Framework Superlattice a. Schematics of synthesis process from left to right, DNA origami synthesis from DNA M13 scaffold (blue) and DNA single stranded staples (orange) into DNA octahedral frames, which then are assembled into a superlattice, growth of silica templated DNA superlattice (red), followed by conversion to SiC via magnesium reduction showing the molybdenum boat, sample and magnesium turnings heated at 660 °C Ar/H₂ for 3 hours with subsequent conversion to silicon carbide (blue). b. Transmission electron microscopy (TEM) Select area electron diffraction (SAED) pattern indexed with (111), (220), and (311) peaks of cubic silicon carbide. c. SEM of low magnification (Left, Scale bar 4μm) and high magnification (Right, Scale bar 500nm) silica

superlattice, d. SEM of SiC region at high magnification (Left, Scale bar, 1 μ m) and low magnification (Right, Scale bar, 5 μ m). e. EDS of SiO₂ superlattice precursor (left) and SiC superlattice (right) with silicon:oxygen atomic ration noted as 2:1 to oxygen signifying conversion to SiC.

2.2 Chemical and Spectroscopic Characterization

To further explore the chemical composition and crystallinity of the converted structure we employed X-ray photoelectron spectroscopy (XPS) and Raman spectroscopy to investigate the surface binding energy and vibrational modes of the created superlattices.

The binding energy of the characteristic silicon 2p peak and carbon 1s peak are both shifted for silicon carbide vs silica.⁵⁸ XPS of the superlattices (**Figure 2a**) shows Si2p peaks at 102.5eV and 100eV before and after Mg reaction, respectively. These positions demonstrate a successful conversion from Si-Ox to Si-C.⁵⁸ This process was accompanied by a shift in the C1s peak from 248.8eV corresponding to adventitious carbon (C-C) bonds to 283 eV after conversion indicating C-Si bonds (Figure 2b). Together the observed peak position changes indicate a formation of SiC, however the broad features of the Si2p suggests a residual Si-Si in the matrix, see Figure S5.

To investigate the details of broad Si2p peak, we employed Raman spectroscopy to probe the crystallinity of the SiC sample. For a SiC-converted batch of superlattices, approximately 20-30 superlattice samples were randomly chosen and examined. Most samples displayed diffuse peaks around 400cm⁻¹ and 800 cm⁻¹ corresponding to small domains of SiC crystallites (Figure 2c).⁵⁹ However, for a portion of the population, approximately 5%, the spectrum displayed a peak between 515-520 nm (Figure 2d) that corresponds to silicon crystallites. This signal was absent from SAED collected via TEM, shown in Figure 1b, which suggests that the silicon phase detected in XPS and Raman consisted of small or amorphous grains.

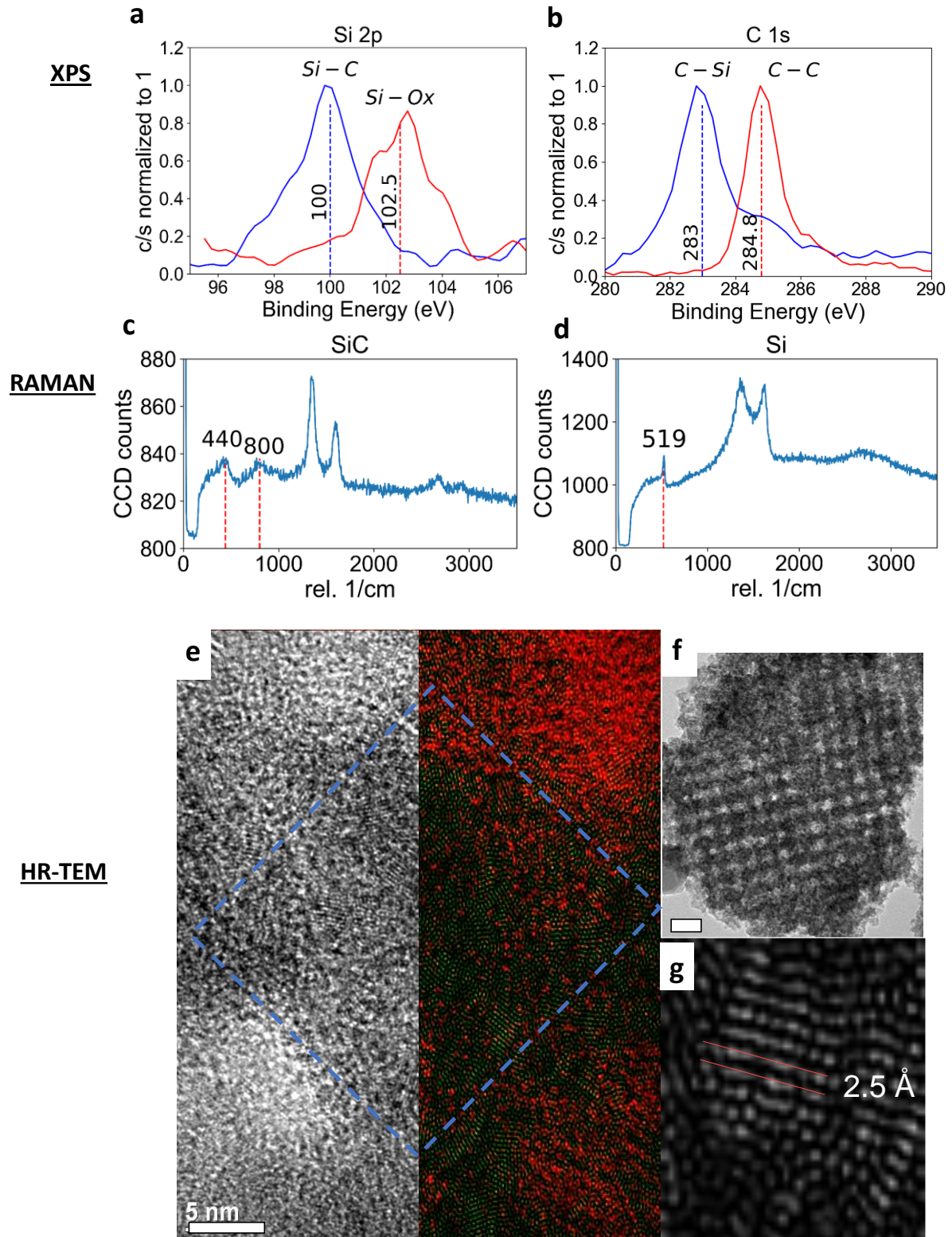


Figure 2. Spectroscopic and structural characterization of SiC superlattice. a) XPS spectra of Si2p peak for silica superlattice (before conversion) in red and SiC superlattice (after conversion) in blue, b) XPS spectra of C1s peak with the 284.8eV adventitious carbon peak in red, the SiC superlattice in blue displays both a C-Si peak at 283 eV and a minor adventitious C-C peak at 284.8eV. c) Raman spectra of superlattices after conversion showing two broad peaks associated with SiC around 400 and 800 rel. 1/cm. d) Raman spectra of superlattice with Silicon peak around 519 rel. 1/cm. e) Left: HRTEM with overlay of an octahedral frame profile, Right: Filtered, false color image with crystalline domains in green with red being the pores, (scale bar 5nm). f) TEM image of a large area lattice array, (scale bar 50nm) g) Fourier filtered domain showing 2.5Å distance indicative of SiC planar spacings of the (111) planes.

To confirm the local composition of the obtained SiC superlattice, we performed a high-resolution (HR)-TEM on a cross section sample that displayed the Raman signals, Figure 2(e-f). The crystalline domains confined to the struts of the octahedron, presented in Figure 2f, have a lattice fringe of 2.5 Å, which corresponds to the d-spacing of (111) planes in SiC. This agrees with the diffraction ring (Figure 1b) for the global structure also measuring 2.5 Å, which corresponds to the SiC-3C polymorph of silicon carbide, a cubic crystal structure with a lattice constant of 4.35 Å. A Fourier filtered image with false coloring in Figure 2d allows us to discern that SiC polycrystalline grains (green) are locally confined to the DNA octahedral frame template with amorphous material, likely Si, filling the rest of the remaining matrix. The size of these SiC crystallites is around 2-5 nm, as revealed by the TEM imaging (Figure S4), which explains the observed broad SiC Raman signal. Based on the XPS results we estimated that the matrix is composed from over 60% the crystalline SiC, 30% of the amorphous silicon and the remaining phosphorous and oxide that were not removed by hydrofluoric acid. Thus, our spectroscopic and

structural studies confirm the formation of SiC framework and provides the detailed information about its composition.

2.3 Electrical Characterization

To evaluate functional characteristics of formed silicon carbide, we performed electrical characterization of the superlattice samples. In order to avoid contamination of the sample, we used an in-situ FIB/SEM electrical testing apparatus which allowed us to limit the use of gallium and platinum that are typically required for sample preparation. Using the sample substrate of molybdenum foil as the common ground, and omniprobe as the source terminal (**Figure 3a**), we measured current-voltage (I-V) characteristics of the converted superlattice sample (5 μ m edge length). To make ohmic contact between the omniprobe and the sample (**Figure 3b-d**) a small amount of platinum (Pt) was deposited to the sample with the Ga ion beam. Shown in the **Figure 3e** is the magnified region of the deposition, which clearly reveal a highly localized Pt with the underlying lattice undisturbed. The I-V curve of converted SiC superlattice was compared against nominal glass, silica formed without DNA in the solution, and silica-superlattices (our pre-conversion material), see **Figure S6**.

The silicon carbide superlattice displayed a resistivity two order of magnitude lower than that of the silica superlattice (**Figure 3f**) and four orders of magnitude lower resistance than sol-gel silica without any DNA. Assuming a simplified geometry of a cube with an edge length of 5 μ m, the resistivity of a SiC superlattice sample was estimated as ~ 3 k ohm-m. This compares against the silica superlattice at ~ 300 k ohm-m and the bulk resistivity of commercial silicon and silicon carbide which doping and purity can result in a spread of 0.01 and >10 k ohm-m, see **Figure 3g** for comparison plot.^{60,61} The small polycrystalline domains of SiC and other impurities likely to contribute to the conductivity of the resulting superlattice, but the reduction of resistivity by a

factor of 100x is a promising indication that future refinement can improve quality of the obtained SiC even further.

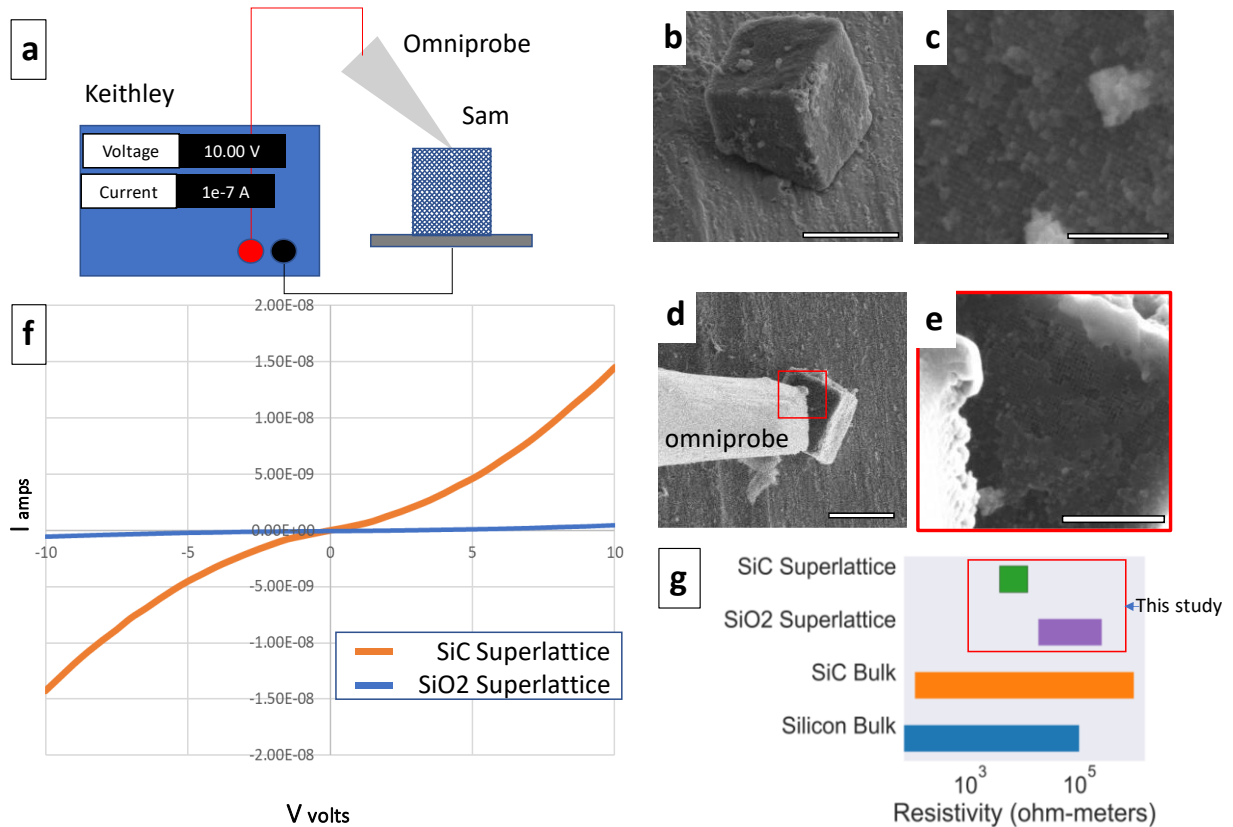


Figure 3. Electrical Characterization of SiC superlattices. a. Keithley, a positive probe running through an omniprobe with ground connecting through the baseplate of the fib/sem stage. b) A SiC superlattice on Mo substrate (scale bar, 4μm), c) High Mag SEM of top surface of the SiC sample before contact (scale bar, 500nm). d) Contacting the sample with the omniprobe, (scale bar, 5μm) e) Higher magnification SEM image of the tip region from (d) showing the preserved nanostructure after securing ohmic contact with Pt, (scale bar 1μm) f) I-V curve sweeping between +/- 10V showing the comparison of SiC superlattices with SiO₂ superlattices. g) A comparison plot for the range of resistivities, with the SiO₂ superlattice in purple,

the SiC superlattice in green alongsize the range associated with SiC bulk in orange and silicon bulk in orange .^{60,61}

3. Conclusion

Here we have demonstrated a new approach for creating of 3D periodic nanoscale SiC superlattices with well-defined architectures. Our approach utilizes a DNA-based self-assembly strategy with further silica templating and conversion into SiC. This approach can be potentially generalized for creating different types of 3D silicon carbide superlattice architectures by leveraging the tailorability of DNA assembly to fabricate different types of lattices and architectures, with or without integration of nanoparticles. The ability to template DNA origami frameworks into SiC replica architecture represents a powerful tool for the creation of potential novel photonic, electronic and mechanical materials. The small size (3-5nm) of the SiC crystallites within the nanoscale framework, shown in our studies, is an encouraging step towards refinement to larger grain growth with application of different annealing methods and high temperature post processing. The results of Raman and XPS measurements also suggest the possibility of refining the synthesis process for optimization of a silicon based nanoarchitectures^{25,57}. Future work would look to further explore, electrical, mechanical, mass transport and thermal properties of these complexly organized 3D frameworks with architected porosity made possible by this fabrication route, and will expand the presented approach to other types of framework nano-architectures.

4. Experimental Section

DNA origami synthesis

In the presented approach we fabricated 3D simple cubic lattice from ~30 nm building blocks, DNA origami.⁵⁶ DNA-origami octahedron frames were synthesized from m13 phage DNA scaffold strands and numerous staple strands. The origami was folded over 20hr in a PCR, and

mixed with its complement in a PCR for an additional 5 days to yield superlattices approximately 5-7 μm in edge length. The structure was characterized using small angle scattering at the CMS beamline to have a lattice constant of 57nm, for further information see Figure S1.

Templated Silica Growth

These superlattices were transferred to a low Mg buffer, converted to silica using an amended sol-gel synthesis of 3-Aminopropyl-triethoxysilane (APTES) and tetraethyl orthosilicate (TEOS) protocol and then drop cast to silicon wafer or molybdenum foil for imaging in the SEM. See Supplemental for more details.

Magnesium Thermal Reduction

In order to convert formed superlattice into silicon carbide, we placed a sample 2-3ul of sample in a molybdenum boat. The sample was then dried in vacuum oven at 80°C for at least 30 minutes. The boat was transferred to the tube furnace adding 10mg Mg turnings either near or directly on top of the sample. The furnace was pumped first to <400mTorr, then backfilled with Ar/4% H₂ and brought to 660°C for 3 hours. Conversion below 650 °C did not yield positive results. Both backfilling the furnace and continuous flowing Ar/4%H₂ led to positive conversion however for consistency a backfilled furnace was used for the experiments.

The resultant sample was removed from the furnace and immersed in 2M HCL for 12 hours to assist in removing MgO and unreacted Mg. To reduce oxygen content further, etching was performed with HF 10:1 Buffered oxide etch solution for 5 minutes or 50:1 BOE for 15-20 minutes. Sample were dried with a nitrogen gun and examined immediately or placed in a desiccator to help reduce dust accumulation. Samples were examined in the Fib/SEM, SEM-EDS,

TEM, Raman, UV-Vis, XPS, and HR-TEM, along with electrical testing, for further details refer to supplemental information.

Supporting Information:

The Supporting Information is available free of charge on the ACS Publications website at DOI: XXXX

Detailed Experimental Conditions, High Resolution TEM, cross-sectional imaging, small angle x-ray scattering (SAXS) and additional figures and discussion.

Acknowledgments:

A.M and H.Z would like to acknowledge Lihua Zhang for assistance with STEM-EDS microscopy, Chang Yong Nam for assisting with experiment design using CFN equipment, Fernando Camino for work related to in-situ electrical conductivity measurements, Xiao Tong and Young Shin for training and discussion of Raman measurements.

This research used resources of the Center for Functional Nanomaterials and the National Synchrotron Light Source II (Complex Material Scattering, beamline 11-ID), which are U.S. DOE Office of Science Facilities, at Brookhaven National Laboratory under Contract No. DE-SC0012704. This research used also the resources of Surface Science Facility in Advanced Science Research Center at Graduate Center of CUNY.

The DNA design work was supported by the US Department of Energy, Office of Basic Energy Sciences, Grant DE-SC0008772. The work was supported by US Department of Defense, Army Research Office, W911NF-19-1-0395.

Conflicts of Interest:

The authors declare no conflict of interest

References

- 1 Bange, R., Bano, E., Rapenne, L., Labau, S., Pelissier, B., Legallais, M., Salem, B. & Stambouli, V. Chemical Stability of Si-SiC Nanostructures under Physiological Conditions. *Materials Science Forum* **897**, 638-641, doi:10.4028/www.scientific.net/MSF.897.638 (2017).
- 2 Zhang, D., Zhao, L. G. & Roy, A. Mechanical Behavior of Silicon Carbide Under Static and Dynamic Compression. *Journal of Engineering Materials and Technology* **141**, doi:10.1115/1.4040591 (2019).

- 3 NEAMȚU, A., Ovezza, D. & NEAMȚU, J. PALLADIUM/SILICON OXIDE/SILICON
CARBIDE NANO-STRUCTURES FOR SENSITIVE DETECTION OF HYDROGEN.
DIGEST JOURNAL OF NANOMATERIALS AND BIOSTRUCTURES **14**, 683-693
(2019).
- 4 Wright, N. G., Horsfall, A. B. & Vassilevski, K. Prospects for SiC electronics and
sensors. *Materials Today* **11**, 16-21, doi:[https://doi.org/10.1016/S1369-7021\(07\)70348-6](https://doi.org/10.1016/S1369-7021(07)70348-6)
(2008).
- 5 Reboredo, F. A., Pizzagalli, L. & Galli, G. Computational Engineering of the Stability
and Optical Gaps of SiC Quantum Dots. *Nano Letters* **4**, 801-804,
doi:10.1021/nl049876k (2004).
- 6 Park, S. H., Park, H., Hur, K. & Lee, S. Design of DNA Origami Diamond Photonic
Crystals. *ACS Applied Bio Materials* **3**, 747-756, doi:10.1021/acsabm.9b01171 (2020).
- 7 Li, Q., Yin, L. & Gao, X. Reduction chemical reaction synthesized scalable 3D porous
silicon/carbon hybrid architectures as anode materials for lithium ion batteries with
enhanced electrochemical performance. *RSC Advances* **5**, 35598-35607,
doi:10.1039/c5ra05342k (2015).
- 8 Li, X., Yan, P., Arey, B. W., Luo, W., Ji, X., Wang, C., Liu, J. & Zhang, J.-G. A stable
nanoporous silicon anode prepared by modified magnesiothermic reactions. *Nano Energy*
20, 68-75, doi:10.1016/j.nanoen.2015.12.011 (2016).
- 9 Zuo, X., Wang, X., Xia, Y., Yin, S., Ji, Q., Yang, Z., Wang, M., Zheng, X., Qiu, B., Liu,
Z., Zhu, J., Müller-Buschbaum, P. & Cheng, Y.-J. Silicon/carbon lithium-ion battery
anode with 3D hierarchical macro-/mesoporous silicon network: Self-templating
synthesis via magnesiothermic reduction of silica/carbon composite. *Journal of Power
Sources* **412**, 93-104, doi:10.1016/j.jpowsour.2018.11.039 (2019).
- 10 Koshida, N. & Matsumoto, N. Fabrication and quantum properties of nanostructured
silicon. *Materials Science and Engineering: R: Reports* **40**, 169-205, doi:10.1016/s0927-
796x(02)00135-3 (2003).
- 11 Jackson, K. M., Dunning, J., Zorman, C. A., Mehregany, M. & Sharpe, W. N.
Mechanical properties of epitaxial 3C silicon carbide thin films. *Journal of
Microelectromechanical Systems* **14**, 664-672, doi:10.1109/JMEMS.2005.847933 (2005).
- 12 Cheng, G., Chang, T.-H., Qin, Q., Huang, H. & Zhu, Y. Mechanical Properties of Silicon
Carbide Nanowires: Effect of Size-Dependent Defect Density. *Nano Letters* **14**, 754-758,
doi:10.1021/nl404058r (2014).
- 13 Hu, P., Dong, S., Zhang, X., Gui, K., Chen, G. & Hu, Z. Synthesis and characterization of
ultralong SiC nanowires with unique optical properties, excellent thermal stability and
flexible nanomechanical properties. *Scientific Reports* **7**, 3011, doi:10.1038/s41598-017-
03588-x (2017).
- 14 Shani, L., Michelson, A. N., Minevich, B., Fleger, Y., Stern, M., Shaulov, A., Yeshurun,
Y. & Gang, O. DNA-assembled superconducting 3D nanoscale architectures. *Nature
communications* **11**, 1-7 (2020).
- 15 Huber, P. Soft matter in hard confinement: phase transition thermodynamics, structure,
texture, diffusion and flow in nanoporous media. *Journal of Physics: Condensed Matter*
27, 103102, doi:10.1088/0953-8984/27/10/103102 (2015).
- 16 Brinker, M., Dittrich, G., Richert, C., Lakner, P., Krekeler, T., Keller, T. F., Huber, N. &
Huber, P. Giant electrochemical actuation in a nanoporous silicon-polypyrrole hybrid
material. *Science Advances* **6**, eaba1483, doi:10.1126/sciadv.aba1483 (2020).

- 17 Sentker, K., Yildirim, A., Lippmann, M., Zantop, A. W., Bertram, F., Hofmann, T., Seeck, O. H., Kityk, A. V., Mazza, M. G., Schönhals, A. & Huber, P. Self-assembly of liquid crystals in nanoporous solids for adaptive photonic metamaterials. *Nanoscale* **11**, 23304-23317, doi:10.1039/C9NR07143A (2019).
- 18 Ross, M. B., Ku, J. C., Vaccarezza, V. M., Schatz, G. C. & Mirkin, C. A. Nanoscale form dictates mesoscale function in plasmonic DNA–nanoparticle superlattices. *Nature nanotechnology* **10**, 453 (2015).
- 19 Martin, H.-P., Ecke, R. & Müller, E. Synthesis of nanocrystalline silicon carbide powder by carbothermal reduction. *Journal of the European Ceramic Society* **18**, 1737-1742 (1998).
- 20 Zhao, B., Zhang, H., Tao, H., Tan, Z., Jiao, Z. & Wu, M. Low temperature synthesis of mesoporous silicon carbide via magnesiothermic reduction. *Materials Letters* **65**, 1552-1555, doi:10.1016/j.matlet.2011.02.075 (2011).
- 21 Su, J., Gao, B., Chen, Z., Fu, J., An, W., Peng, X., Zhang, X., Wang, L., Huo, K. & Chu, P. K. Large-Scale Synthesis and Mechanism of β -SiC Nanoparticles from Rice Husks by Low-Temperature Magnesiothermic Reduction. *ACS Sustainable Chemistry & Engineering* **4**, 6600-6607, doi:10.1021/acssuschemeng.6b01483 (2016).
- 22 Bao, Z., Weatherspoon, M. R., Shian, S., Cai, Y., Graham, P. D., Allan, S. M., Ahmad, G., Dickerson, M. B., Church, B. C., Kang, Z., Abernathy, H. W., 3rd, Summers, C. J., Liu, M. & Sandhage, K. H. Chemical reduction of three-dimensional silica micro-assemblies into microporous silicon replicas. *Nature* **446**, 172-175, doi:10.1038/nature05570 (2007).
- 23 Klein, S., Winterer, M. & Hahn, H. Reduced-pressure chemical vapor synthesis of nanocrystalline silicon carbide powders. *Chemical Vapor Deposition* **4**, 143-149 (1998).
- 24 Anma, H., Yoshimoto, Y., Warashina, M. & Hatanaka, Y. Low temperature deposition of SiC thin films on polymer surface by plasma CVD. *Applied surface science* **175**, 484-489 (2001).
- 25 Dorval Courchesne, N.-M., Steiner III, S. A., Cantú, V. J., Hammond, P. T. & Belcher, A. M. Biotemplated silica and silicon materials as building blocks for micro-to nanostructures. *Chemistry of Materials* **27**, 5361-5370 (2015).
- 26 Boles, M. A., Engel, M. & Talapin, D. V. Self-Assembly of Colloidal Nanocrystals: From Intricate Structures to Functional Materials. *Chemical Reviews* **116**, 11220-11289, doi:10.1021/acs.chemrev.6b00196 (2016).
- 27 Majewski, P. W., Rahman, A., Black, C. T. & Yager, K. G. Arbitrary lattice symmetries via block copolymer nanomeshes. *Nature Communications* **6**, 7448, doi:10.1038/ncomms8448 (2015).
- 28 Shevchenko, E. V., Talapin, D. V., Kotov, N. A., O'Brien, S. & Murray, C. B. Structural diversity in binary nanoparticle superlattices. *Nature* **439**, 55-59, doi:10.1038/nature04414 (2006).
- 29 Shi, Y., Zhang, F., Hu, Y.-S., Sun, X., Zhang, Y., Lee, H. I., Chen, L. & Stucky, G. D. Low-Temperature Pseudomorphic Transformation of Ordered Hierarchical Macromesoporous SiO₂/C Nanocomposite to SiC via Magnesiothermic Reduction. *Journal of the American Chemical Society* **132**, 5552-5553, doi:10.1021/ja1001136 (2010).
- 30 Hatton, B., Mishchenko, L., Davis, S., Sandhage, K. H. & Aizenberg, J. Assembly of large-area, highly ordered, crack-free inverse opal films. *Proceedings of the National Academy of Sciences* **107**, 10354, doi:10.1073/pnas.1000954107 (2010).

- 31 Rahman, A., Majewski, P. W., Doerk, G., Black, C. T. & Yager, K. G. Non-native three-dimensional block copolymer morphologies. *Nature Communications* **7**, 13988, doi:10.1038/ncomms13988 (2016).
- 32 Nghiem, Q. D., Kim, D.-P. & Kim, S. O. Well-Ordered Nanostructure SiC Ceramic Derived from Self-Assembly of Polycarbosilane-Block-Poly(methyl methacrylate) Diblock Copolymer. *Journal of Nanoscience and Nanotechnology* **8**, 5527-5531, doi:10.1166/jnn.2008.1285 (2008).
- 33 Beaucage, P. A., Susca, E. M., Gruner, S. M. & Wiesner, U. B. Discovering Synthesis Routes to Hexagonally Ordered Mesoporous Niobium Nitrides Using Poloxamer/Pluronic Block Copolymers. *Chemistry of Materials* **29**, 8973-8977, doi:10.1021/acs.chemmater.7b03834 (2017).
- 34 She, Y., Goodman, E. D., Lee, J., Diroll, B. T., Cargnello, M., Shevchenko, E. V. & Berman, D. Block-Co-polymer-Assisted Synthesis of All Inorganic Highly Porous Heterostructures with Highly Accessible Thermally Stable Functional Centers. *ACS Applied Materials & Interfaces* **11**, 30154-30162, doi:10.1021/acsami.9b09991 (2019).
- 35 Berman, D. & Shevchenko, E. Design of functional composite and all-inorganic nanostructured materials via infiltration of polymer templates with inorganic precursors. *Journal of Materials Chemistry C* **8**, 10604-10627, doi:10.1039/D0TC00483A (2020).
- 36 Tian, Y., Zhang, Y., Wang, T., Xin, H. L., Li, H. & Gang, O. Lattice engineering through nanoparticle-DNA frameworks. *Nat Mater* **15**, 654-661, doi:10.1038/nmat4571 (2016).
- 37 Lin, Z., Emamy, H., Minevich, B., Xiong, Y., Xiang, S., Kumar, S., Ke, Y. & Gang, O. Engineering Organization of DNA Nano-Chambers through Dimensionally Controlled and Multi-Sequence Encoded Differentiated Bonds. *Journal of the American Chemical Society* **142**, 17531-17542 (2020).
- 38 Wang, P., Gaitanaros, S., Lee, S., Bathe, M., Shih, W. M. & Ke, Y. Programming self-assembly of DNA origami honeycomb two-dimensional lattices and plasmonic metamaterials. *Journal of the American Chemical Society* **138**, 7733-7740 (2016).
- 39 Tian, Y., Wang, T., Liu, W. Y., Xin, H. L., Li, H. L., Ke, Y. G., Shih, W. M. & Gang, O. Prescribed nanoparticle cluster architectures and low-dimensional arrays built using octahedral DNA origami frames. *Nature Nanotechnology* **10**, 637-+, doi:10.1038/nnano.2015.105 (2015).
- 40 Ma, N. N., Minevich, B., Liu, J. L., Ji, M., Tian, Y. & Gang, O. Directional Assembly of Nanoparticles by DNA Shapes: Towards Designed Architectures and Functionality. *Topics in Current Chemistry* **378**, doi:10.1007/s41061-020-0301-0 (2020).
- 41 Jun, H., Shepherd, T. R., Zhang, K., Bricker, W. P., Li, S., Chiu, W. & Bathe, M. Automated Sequence Design of 3D Polyhedral Wireframe DNA Origami with Honeycomb Edges. *ACS Nano* **13**, 2083-2093, doi:10.1021/acs.nano.8b08671 (2019).
- 42 Sutter, E., Zhang, B. & Sutter, P. DNA-Mediated Three-Dimensional Assembly of Hollow Au-Ag Alloy Nanocages as Plasmonic Crystals. *ACS Applied Nano Materials* **3**, 8068-8074, doi:10.1021/acsanm.0c01528 (2020).
- 43 Rothmund, P. W. Folding DNA to create nanoscale shapes and patterns. *Nature* **440**, 297 (2006).
- 44 Douglas, S. M., Marblestone, A. H., Teerapittayanon, S., Vazquez, A., Church, G. M. & Shih, W. M. Rapid prototyping of 3D DNA-origami shapes with caDNAno. *Nucleic acids research* **37**, 5001-5006 (2009).

- 45 Tian, Y., Lhermitte, J. R., Bai, L., Vo, T., Xin, H. L., Li, H., Li, R., Fukuto, M., Yager, K. G. & Kahn, J. S. Ordered three-dimensional nanomaterials using DNA-prescribed and valence-controlled material voxels. *Nature Materials*, 1-8 (2020).
- 46 Liu, W., Tagawa, M., Xin, H. L., Wang, T., Emamy, H., Li, H., Yager, K. G., Starr, F. W., Tkachenko, A. V. & Gang, O. Diamond family of nanoparticle superlattices. *Science* **351**, 582-586 (2016).
- 47 Senesi, A. J., Eichelsdoerfer, D. J., Macfarlane, R. J., Jones, M. R., Auyeung, E., Lee, B. & Mirkin, C. A. Stepwise Evolution of DNA-Programmable Nanoparticle Superlattices. *Angewandte Chemie* **125**, 6756-6760 (2013).
- 48 Oh, T., Ku, J. C., Lee, J. H., Hersam, M. C. & Mirkin, C. A. Density-Gradient Control over Nanoparticle Supercrystal Formation. *Nano Lett* **18**, 6022-6029, doi:10.1021/acs.nanolett.8b02910 (2018).
- 49 Lewis, D. J., Zornberg, L. Z., Carter, D. J. D. & Macfarlane, R. J. Single-crystal Winterbottom constructions of nanoparticle superlattices. *Nat Mater* **19**, 719-724, doi:10.1038/s41563-020-0643-6 (2020).
- 50 Pal, S., Zhang, Y. G., Kumar, S. K. & Gang, O. Dynamic Tuning of DNA-Nanoparticle Superlattices by Molecular Intercalation of Double Helix. *Journal of the American Chemical Society* **137**, 4030-4033, doi:10.1021/ja512799d (2015).
- 51 Jia, S., Wang, J., Xie, M., Sun, J., Liu, H., Zhang, Y., Chao, J., Li, J., Wang, L., Lin, J., Gothelf, K. V. & Fan, C. Programming DNA origami patterning with non-canonical DNA-based metallization reactions. *Nature Communications* **10**, 5597, doi:10.1038/s41467-019-13507-5 (2019).
- 52 Nguyen, L., Döblinger, M., Liedl, T. & Heuer-Jungemann, A. DNA-Origami-Templated Silica Growth by Sol–Gel Chemistry. *Angewandte Chemie International Edition* **58**, 912-916, doi:10.1002/anie.201811323 (2019).
- 53 Liu, X., Zhang, F., Jing, X., Pan, M., Liu, P., Li, W., Zhu, B., Li, J., Chen, H., Wang, L., Lin, J., Liu, Y., Zhao, D., Yan, H. & Fan, C. Complex silica composite nanomaterials templated with DNA origami. *Nature* **559**, 593-598, doi:10.1038/s41586-018-0332-7 (2018).
- 54 Keren, K., Berman, R. S. & Braun, E. Patterned DNA Metallization by Sequence-Specific Localization of a Reducing Agent. *Nano Letters* **4**, 323-326, doi:10.1021/nl035124z (2004).
- 55 Li, Z., Liu, L., Zheng, M., Zhao, J., Seeman, N. C. & Mao, C. Making Engineered 3D DNA Crystals Robust. *Journal of the American Chemical Society* **141**, 15850-15855, doi:10.1021/jacs.9b06613 (2019).
- 56 Tian, Y., Lhermitte, J. R., Bai, L., Vo, T., Xin, H. L. L., Li, H. L., Li, R. P., Fukuto, M., Yager, K. G., Kahn, J. S., Xiong, Y., Minevich, B., Kumar, S. K. & Gang, O. Ordered three-dimensional nanomaterials using DNA-prescribed and valence-controlled material voxels. *Nature Materials*, doi:10.1038/s41563-019-0550-x (2020).
- 57 Entwistle, J., Rennie, A. & Patwardhan, S. A review of magnesiothermic reduction of silica to porous silicon for lithium-ion battery applications and beyond. *Journal of Materials Chemistry A* **6**, 18344-18356, doi:10.1039/c8ta06370b (2018).
- 58 Rumble Jr, J., Bickham, D. & Powell, C. The NIST x-ray photoelectron spectroscopy database. *Surface and interface analysis* **19**, 241-246 (1992).
- 59 Colomban, P.
- 60 Accuratus. *Silicon Carbide, SiC Ceramic Properties*, (2020).

61 HAAS, R. *CVD Silicon Carbide*, 2020).